International Journal of Nanoelectronics and Materials
IJNeaM
ISSN 1985-5761 | E-ISSN 2232-1535

Review of Indium Oxide Based on Different Applied Methods

Qamar Q Mohammed[a], Sarmad Fawzi Hamza Alhasan[b], Zaid T. Salim[c], Reem M. Khalaf[d], Makram A. Fakhri[e,*], A. Mindil[f], Motahher A. Qaeed[f], Subash C. B. Gopinath[f, g, h], Ahmed A. Al-Amiery[i],

[a]*College of Control Engineering, University of Technology-Iraq, Baghdad, Iraq*
[b]*Collage of Communication Engineering, University of Technology-Iraq, Baghdad, Iraq*
[c]*College of Energy and Environmental Sciences, Al-Karkh University of Science, Baghdad 10081, Iraq*
[d]*Al-Farahidi University, Baghdad, Iraq*
[e]*College of Laser and Optoelectronic Engineering, University of Technology-Iraq, Baghdad, Iraq*
[f]*Department of Physical Sciences, Faculty of Science, University of Jeddah, Jeddah, Saudi Arabia*
[g]*Center for Global Health Research, Saveetha Medical College & Hospital Saveetha Institute of Medical and Technical Sciences (SIMATS), Thandalam, Chennai – 602 105, Tamil Nadu, India*
[h]*Faculty of Chemical Engineering & Technology and Institute of Nano Electronic Engineering, Universiti Malaysia Perlis (UniMAP), 02600 Arau, Perlis, Malaysia*
[i]*Department of Technical Sciences, Western Caspian University, Baku AZ 1075, Azerbaijan.5Al-Mustaqbal University College, Department of Medical Physics, Iraq*
[j]*Al-Ayen Scientific Research Center, Al-Ayen Iraqi University, AUIQ, P.O. Box: 64004, An Nasiriyah, Thi Qar, Iraq*
**Corresponding author. Tel.: +964y7702793869; e-mail: Makram.a.fakhri@uotechnology.edu.iq, mokaram_76@yahoo.com*

ABSTRACT

This article examines the characteristics of In2O3 thin films produced using various deposition techniques. The stability of an aqueous solution containing indium at different concentrations was assessed. Thermo-gravimetric and differential thermal analyses were conducted on the desiccated sol particles to gain a deeper understanding of the thermal processes that occur during sintering. The microstructure, phase purity, and optical properties of thin films produced through various deposition techniques such as dip-coating on glass substrates were analyzed using transmission electron microscopy, x-ray diffractometry, and visible light spectrometry. The variations in morphology among the different systems were used to explain the differences in optical properties observed in the films.

Keywords: *Bio-sensors, Electrochemical sensors, Indium Oxide, Nanostructure, Nano-films*

1. INTRODUCTION

In2O3 is a conductive material with a wide bandgap (3.5 eV–3.75 eV) and crystalline structure. The optical bandgap of nanostructured In2O3 is notably shifted towards the blue when compared to bulk In2O3. The morphology of nano-sized In2O3 particles is spherical, and their specific surface area (SSA) ranges from 25-50 m2/g. In addition to this, high purity, coated, and dispersed nano In2O3 particles are also obtainable [1-4].

Various forms of In2O3 nanostructures have been fabricated using methods with different techniques such as chemical vapor deposition, spray pyrolysis, vacuum evaporation, and magnetron sputtering can be employed for the deposition of In2O3 thin films [5-8].

Inkjet printing, atomic layer deposition, physical vapor deposition by sputtering, and chemical spray pyrolysis are some of the methods used for the production of In2O3 thin films and pulsed laser deposition have several advantages, such as stoichiometric control, multi-layered thin films, and control over morphology and crystallinity [9-13].

In2O3 -based nanostructured thin films have exceptional optical, electrical, and mechanical properties that make them significant in various applications including but not limited to energy conversion, biological and chemical sensing, solar cells, and thin-film transistors due to their unique properties and characteristics. [14–22]. In2O3 is also used in biosensors for detection and as a photodiode due to its high sensitivity to UV light. In2O3 nanostructures have high sensitivity, selectivity, and stability for use as chemical and biological sensors [23-26]. Recently, studies have been conducted on the fabrication of In2O3 nanostructures in various forms.

1.1 Crystal Structure

Indium oxide (In2O3) commonly adopts a stable bixbyite structure, where the lattice parameter a equals 10.117 Å. This structure comprises 16 formula units present in a single cubic unit cell and 80 atoms, with 8 formula units and 40 atoms in the primitive unit cell [27-30]. The bixbyite structure results from the removal of 1/4 of the oxygen atoms from a 2 × 2 × 2 fluorite structure and after the initial formation of the lattice structure, there is subsequent relaxation of atom positions. Within the lattice, indium atoms occupy two distinct non-equivalent positions [31-34]. Coordinated by Oxygen atoms are arranged in both octahedral and trigonal prismatic configurations [35, 36].

In addition to the stable crystal structure, a meta-stable rhombohedral polymorph (space group 167, R c3) has also been observed in nanostructures or achieved through epitaxial growth on c-plane sapphire substrates with specific conditions. This polymorph has lattice parameters a = 5.487 Å, c = 14.510 Å and contains two formula units (ten atoms) per primitive unit cell. However, this polymorph is not the focus of this review paper [18, 20, and 37-39]. Figure 1 presents the stable crystal structure, and a meta-stable cubic and rhombohedral polymorph depicts the bixbyite structure.

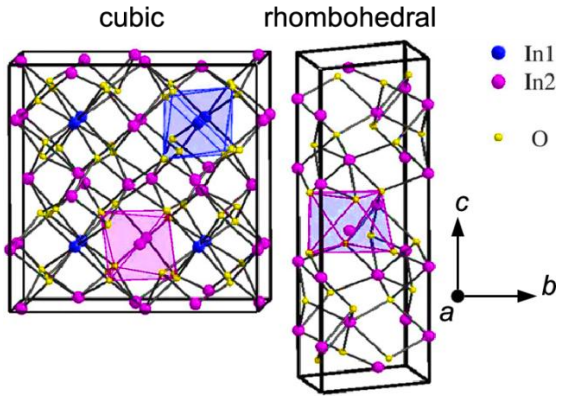

Figure 1. The stable crystal structure (cubic) and a meta-stable rhombohedral polymorph for indium oxide.

The crystal structure of In2O3 includes a stable cubic bixbyite and a metastable rhombohedra polymorph, which are depicted in Figure 1. In the figure, the different coordination of in is highlighted with different colors.

1.2 Synthesis

To utilize In2O3 as a semiconductor with the same potential as Si, GaAs, or GaN, it is crucial to utilize strategies of expansion that ensure superior crystal quality and purity, and keep unintended dopant impurities to a minimum. In2O3 single crystals in bulk serve as the fundamental material for investigating the band structure via angular resolved photoelectron spectroscopy, as well as being the basic material used to make single-crystalline substrates. These substrates provide the foundation for optimal homoepitaxial material quality In2O3 thin films, which have fewer long-term flaws than those developed on non-native substrates that don't match the lattice. The application of exceedingly pure, self-seeded In2O3 crystals formed from the indium and oxygen vapor phases at 1000°C by weiher produced needle-shaped single crystals (5 × 0.5 × 0.5 mm).

Transport of chemical vapors with In2O3 as the source material and Iodine and sulfur as modes of transfer agents has yielded slightly larger self-seeded In2O3 single crystals (typically 3 × 3 × 1 mm). However, the high concentration of unintentional electrons in these crystals imply the inclusion of transport agents, in addition to other donor impurities. Huge single crystals that can be used to make substrates (cm2 × mm) were grown using the flux technique with Flux agents B2O3, PbO, and MgO. Unfortunately, these crystals also suffer from the inclusion of unintentional impurities such as Mg and Pb. A recent innovative growth technique [28] used to melt grow In2O3 provided cm3 single crystals appropriate for substrate production having a high degree of purity and a low level of accidental electron concentration [24, 40-44]. To attain behavior that is semi-insulating or extremely conductive, suitable substrate doping is required by electron transport devices that relies on horizontal or vertical transport, accordingly [45, 46].

1.3 Transparency to Visible Light, Band Structure, and Effective Electron Mass

In the ultraviolet range, indium oxide has strong optical absorption and is transparent to visible light, with a direct band gap of approximately 3.7 eV, which was previously mistakenly referred to as In2O3's basic band gap. A lower absorption, which prevents the blue section of the visible spectrum in bulk or heavy films, was initially considered a 2.6 eV indirect band gap with the maximal valence band (VBM) distant from the Γ-point. A thin film's absorption spectrum (a) and a thick bulk sample, where the lack of absorption is more noticeable (b), corresponding to this. X-ray experiments using photoelectron spectroscopy (XPS) have recently contested the commonly reported band gap value of around 3.7 eV based on optical absorption in thin films and corrected its value to be between 2.7-2.9 eV.

1.4 Growth and Characterization of Indium Oxide

The objective of our study is to examine the formation of indium oxide nanoparticles on a porous silicon substrate utilizing pulsed laser deposition (PLD) and investigate their characteristics by X-ray diffraction (XRD) analysis. We have adapted the Diffraction of X-rays (XRD) test, atomic force microscopy (AFM), and photoluminescence (PL) to study the optical properties (intrinsic and extrinsic) and determine the lattice constant of various crystalline surface materials. Additionally, field emission scanning electron microscopy (FESEM) with a large depth of field will be employed to obtain information about the topography and constituent elements at magnifications ranging from 10x to 300,000x.

1.5 Doping of Indium Oxide

As a comparison between the pure Indium oxide and the doped one, doping is used to obtain a new working wavelength during the device's manufacturing that could not be found in the original material (indium oxide) or other material individually. This unique wavelength will be different, and the doping process will impact the work area from various angles and effect on the particle size.

Table 1 In2O3 Nano Films Biosensors

Year	Analyte	Material	Method	Result
2019 [24]		In_2O_3 thin films	Rapid photonic curing	
2019 [28]	Water	amorphous In2O3:H films	Electron energy loss spectroscopy	Metallic indium in UHV at a greater temperature
2019 [30]	Glucose and urea sensing	EIS biosensors based on In_2O_3 and In2TiO5	CF4 therapy after plasma	59.64 mV/pH sensitivity and 99.68% linearity
2020 [31]	pH	In_2O_3 nanoribbon on polyethylene terephthalate (PET)	Shadow mask patterning	The thickness of 1.4 mm and sensitivity of 4 U/C
2020 [39]		Non-carbon 2D black phosphorous, phosphorene, semiconductor transition metal dichalcogenides, and 2D metal oxides		Large transconductance and high sensitivity
2020 [40]	Artificial tears, sweat, and saliva and electrical sensing data capture	TFTs based on In_2O_3 nanoribbons with co-planar reference electrodes, Au		Surface complexation at all levels, excellent chemical stability in salt solutions with several receptors and large transconductance for high sensitivity
2020 [41]	SARS, MERS, COVID-19 and DNA sensor	Graphene and In_2O_3 nanowires		Excellent sensitivity, selectivity, and low detection limits
2021 [37]	Cardiac troponin (cTnI)	Au/In_2O_3 nanocubes as label-free aptasensors		Detection threshold of 0.06 ng/ml and wide linear range of 0.1-1000 ng/mland high analytical selectivity
2021 [38]	pH	In_2O_3 -EGTFTs		The pH sensitivity 64 mV/pH with a deviation of 10 mV
2021 [43]	DNA	In_2O_3 nanowire FET		VTH with an average repeatability of 5.235 V and a standard deviation of 0.382 V
2022 [23]	mRNA SARS-CoV-2	Gold, silver, graphene, In_2O_3 nanowire, iron oxide, quantum dots, and carbon nanofibers are examples of materials.		Reduce the mortality brought on by coronaviruses
2022 [25]	Glucose	In_2O_3 nanoribbon FET		Enhanced the detection sensitivity and shortened the detection time
2022 [26]	Ethanol in aqueous samples with CCD-RSM	Graphene-indium oxide		Detection limit 0.068 mol/L, and linear response up to 1.2 mol/L
2022 [27]		Sn-doped In_2O_3 NCs		LSPR energy (1100 cm-1) and extinction (over 300% enhancement)
2022 [29]	SARS-CoV-2	In_2O_3 nanoribbon field-effect transistor (FET)	Tinny shadow mask	UTM (LoD: 100 fg/mL) and S1 protein-specific IgG antibody

				(LoD: 1 pg/mL) in human whole blood
2022 [42]	DNA, prostate cancer antigen, glucose, dopamine, p24 protein, PlGF protein, cardiac troponin I (cTnI), creatine kinase MB, and B-type natriuretic peptide, and cholesterol are all involved.	In_2O_3 nanoribbon field-effect transistor (FET)		A range of detection of 4–9 (pH) fg-g
2023 [43]	NO_2	PANI-doped In_2O_3 nanosheets	Hydrothermal technique	The nanostructures not only deplete electrons in the PANI-incorporated materials, but also provide a large number of surface adsorption sites and effective gas diffusion paths. The as-synthesized In_2O_3/PANI-1 sensors have extremely high responses (341.5 @ 30 ppm, 12.8 @ 3 ppm) to NO_2 gas at a working temperature (250 °C), quick response times (24 s @ 30 ppm, 47 s @ 3 ppm) and recovery times (53 s @ 30 ppm, 74 s @ 3 ppm), and a low detection limit (300 ppb). high repeatability and selectivity
2023 [44]	Detection H_2S	In_2O_3/ZnO	One-step co-precipitation method followed by thermal annealing in air.	The gas sensing performance test results of the In_2O_3/ZnO hollow nanocages show that their response to H_2S gas is significantly improved 67.5 @50 ppm H_2S (about 11 times that of pure ZnO nanocages) at an optimal temperature of 200 °C, better selectivity, lower theoretical detection limit and good linearity between gas concentration and response values
2023 [45]	Uv-enhanced formaldehyde sensor	Hollow In_2O_3@TiO_2 double-layer	Facile water bath method using the sacrifice template of carbon nanospheres.	The response of the In_2O_3/TiO_2 nanocomposite-based sensor to 1 ppm formaldehyde is about 3.8, and the response time and recovery time are 28 and 50 s, respectively. The detectable formaldehyde concentration can reach as low as 0.06 ppm. The enhanced sensing properties of In2O3/TiO2 nanocomposites are attributed to nanoheterojunctions between the components and the combined photocatalytic effects under UV-light-emitting diode irradiation, as supported by density functional theory calculations

2023 [46]	Conductometric isopropanol gas sensor	In2O3 nanosheets and Ce doped In2O3 hierarchical microstructures	Hydrothermal	In_2O_3 nanosheets exhibited the highest sensing response (93), which was 6 times higher than that of the pristine In_2O_3 towards 100 ppm isopropanol at the optimized working temperature of 220 °C. Furthermore, the Ce-In_2O_3 samples showed short response and recovery time, high selectivity, broad dynamic range and acceptable long-term stability
2023 [47]	Ethanol detection	Sandwich-structured $IN_2S_3/IN_2O_3/IN_2S_3$ hollow nanofibers	An electrospinning technique combining with postvulcanization treatments.	the ISOS HNF sensors show a high response improved by 23% and 76% compared to those of the In_2S_3/In_2O_3 core–shell NF and In_2O_3 HNF ones, respectively. Moreover, the ISOS HNF sensors also exhibit a fast response/recovery rate (<1 s/25 s) and a good gas selectivity property. The significant improvement in response is attributed to the double In2S3/In2O3 heterointerfaces and increased O vacancies, while the accelerated response/recovery rate is due to the double-constructed heterojunction and suitable mesopores in the coatings, and the enhanced gas selectivity is due to the In2S3 shell

1.6 Temperature Effect on Indium Oxide

It was found that increasing the calcination temperature between 200 and 300°C reduced the dimensions of In2O3 nanoparticles. At 300 °C, the entire transformation of In(OH)3 NPs to In2O3 NPs occurred. The temperature of calcination is a critical element in developing In2O3 NPs with various structures, size distributions, and morphologies. The increased crystallite size and crystallinity of In2O3 calcined nanoparticles temperatures demonstrate that crystallite growth is enhanced at higher calcination temperatures.

1.7 Thickness Effect of Indium Oxide

The thickness of the outer layer of the In2O3 target is affected by the laser wavelength (deposition process). Decreasing the outer layer thickness will cause a decrease in the regularity of the distribution of the crystal. The threshold voltage of these devices (VTH) tends to gravitate toward more negative possibilities when the channel thickness grows due to increased free carriers. In contrast, the impact of the field on mobility (μFE) varies with the consistency of single layers. It improved in ZnO TFTs using thicker sheets and demonstrated degenerative behavior for In2O3 further research is needed on films thicker than 11.5 nm.

1.8 The Applied Method of In2O3

We used PLD (pulsed laser deposition) as a physical vapor deposition (PVD) technique. To deposit the material (In2O3) on a target, a high-intensity pulsed laser beam is focused inside a vacuum chamber. We made use of it because of its many benefits. At low substrate temperatures and a quick growth rate of the order of pulse, thin films can be grown in a high vacuum to produce stoichiometric films. Additionally, they are particularly advantageous for materials with complex chemical compositions, combinatorial maps, readily available multi-layered thin films, adhesive coatings, excellent flexibility in experimental design, and control over morphology and crystallinity. Furthermore, altering the deposition conditions allows further customization of the coatings' composition-structure-properties relationship.

1.8.1 Nd: YAG Laser in Pulsed Laser Deposition

We used Nd: YAG lasers (neodymium-doped yttrium aluminum garnet) because have several advantages over other types of lasers for PLD. For example, they are relatively inexpensive, easy to operate, and have high beam quality and stability. They can also be used to deposit a wide range of materials, including metals, ceramics, and polymers. The use of Nd: YAG lasers in PLD is a powerful tool for the fabrication of high-quality thin films with a wide range of applications in electronics, optics, and energy.

1.9 Optical Applications of In2O3

In2O3 nanoparticles are used for several applications and have been used effectively for susceptible Thin film transistors (TFTs), chemical sensors, biosensors, optical detectors, and solar cells [35], Indium oxide in biosensors for various applications is easy to study and manufacture, such as the investigation of biomolecules and their interactions, the pharmaceutical manufacturing and organ replacement, environmental fiel monitoring, industrial process monitoring, detection of crime, health technologies, tissue engineering, and regenerative medicine, and food analysis, medical diagnosis (both clinical and laboratory use), etc.

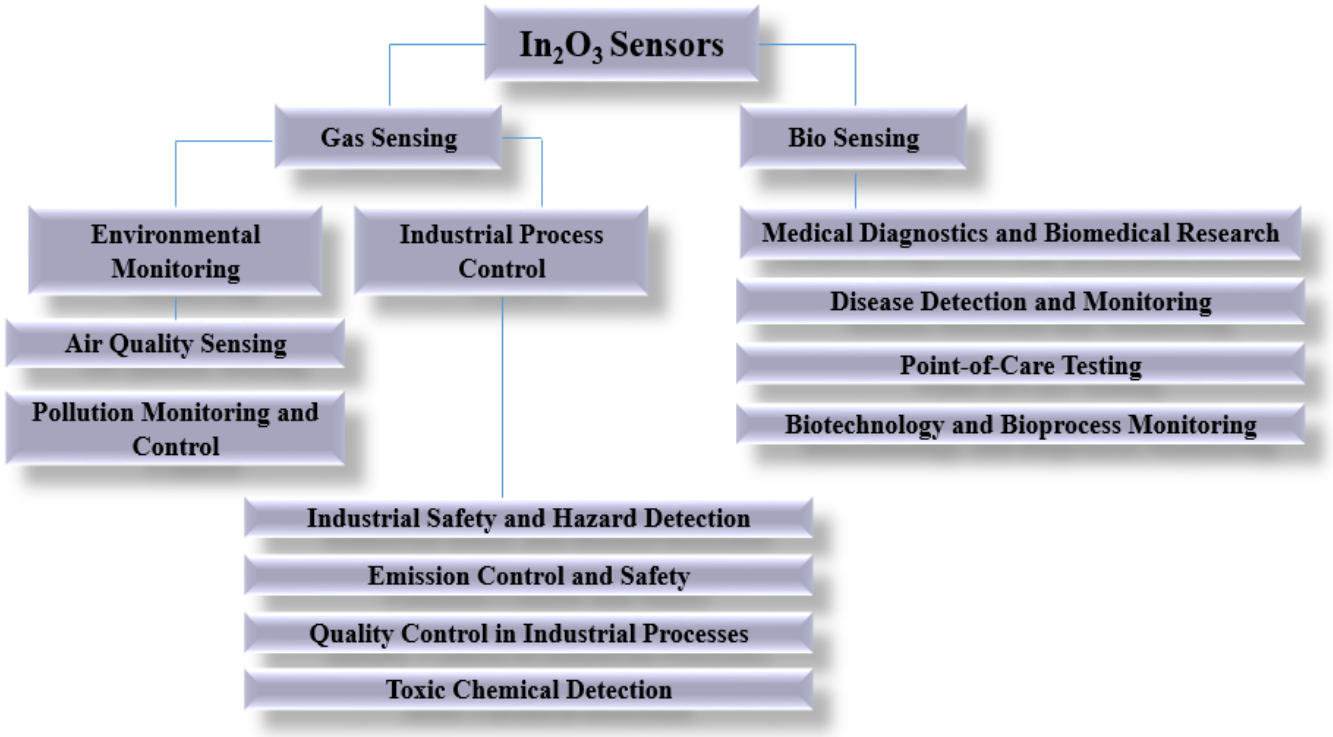

Figure 2. Schematic diagram of In2O3 Sensors applications.

Figure 2 illustrated that In2O3 is used in a variety of sensing contexts, such as chemical, biological, gas, and environmental monitoring. It is furthermore utilized in industrial process control to guarantee effectiveness and safety. In2O3 is a useful material in a variety of sectors and scientific research due to its adaptability. The most important type of In2O3 sensor depends on the contexts and the specific needs of the industry or the field it serves. Each application addressed a unique challenges and contributes to improve the quality of life, safety and the advancements in the various fields of life.

1.9.1 Biosensors

Biosensors are analytical devices that utilize biological recognition elements to detect and quantify specific analytes. They typically consist of three main components: the biological recognition element, the transducer, and the signal processor.

Biological recognition element: This is a biomolecule that selectively binds to the analyte of interest. Examples of biological recognition elements include enzymes, antibodies, nucleic acids, and whole cells.

Transducer: This component converts the biological recognition event into a measurable signal. Common transducer types include optical, electrochemical, and piezoelectric transducers.

Signal processor: This component amplifies, filters, and analyzes the signal generated by the transducer to provide a quantitative measurement of the analyte.

The principle of operation of a biosensor involves the specific interaction between the biological recognition element and the target analyte. This interaction leads to a change in the physicochemical properties of the biological recognition element, which in turn generates a signal that is transduced by the transducer. The signal generated by the transducer is proportional to the amount of analyte present in the sample. The signal is then processed and converted into a quantitative measurement of the analyte concentration.

Overall, biosensors offer a rapid, sensitive, and selective means of detecting and quantifying analytes in various fields, including medical diagnosis, environmental monitoring, and food safety.

1.9.2 Biosensors That Used In2O3

Indium oxide (In2O3) is a semiconducting metal oxide material that has been widely used as a transducer material in biosensors. The main types of biosensors that utilize In2O3 are:

1. Electrochemical biosensors: These biosensors rely on the changes in the electrical properties of In2O3 due to the interaction with the analyte. The electrical properties can be measured by techniques such as impedance spectroscopy or cyclic voltammetry.
2. Optical biosensors: These biosensors use In2O3 as a transducer material for surface plasmon resonance (SPR) or surface-enhanced Raman spectroscopy (SERS) techniques. The change in the refractive index or the Raman signal due to the interaction of the analyte with the immobilized biomolecules on the surface of In2O3 is measured.
3. Gas sensors: In2O3 can also be used in gas sensors due to its high sensitivity and selectivity towards specific gases. The interaction between In2O3 and the gas analyte can cause a change in the electrical conductivity, which can be measured.

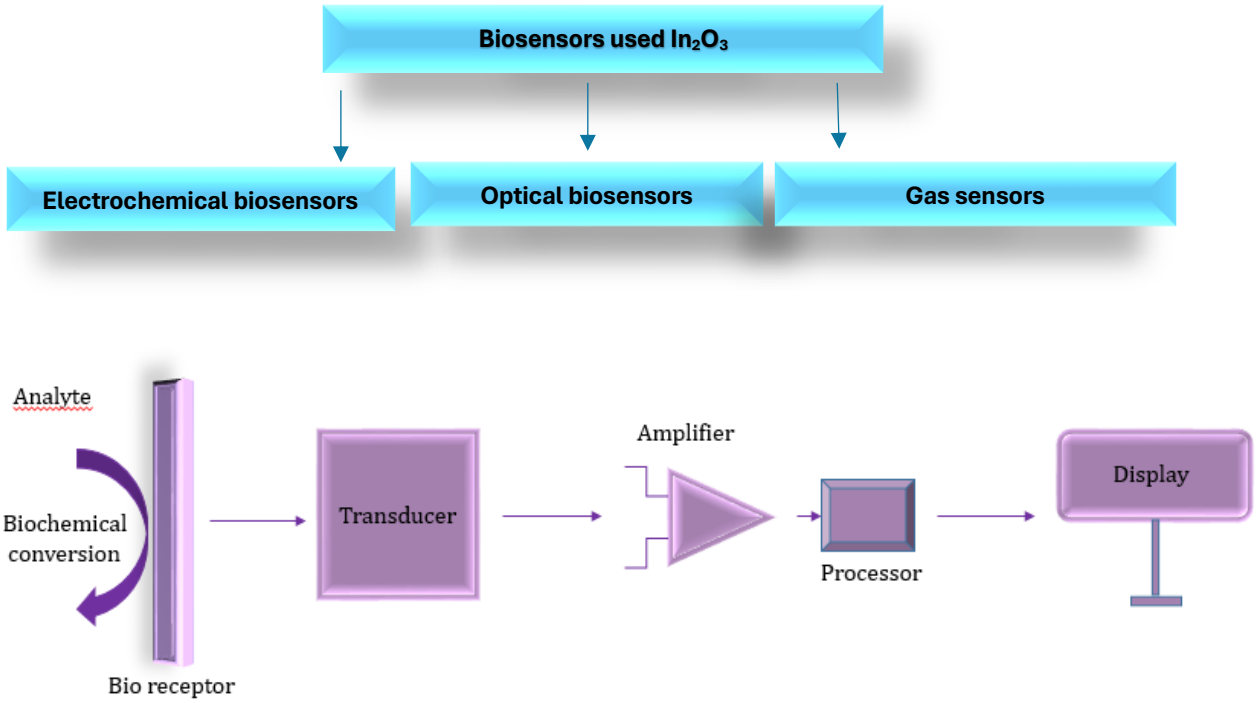

Figure 3. Schematic diagram of typical biosensor consisting of bioreceptor, transducer, electronic system (amplifier and processor), and display (PC or printer).

2. CONCLUSION

This article provides an overview of the potential applications and semiconductor properties of In2O3, a wide-band gap material. It discusses the high-purity single-crystal synthesis required for the development of semiconducting devices and highlights the sudden availability of large quantities of In2O3 substrates which allow for the highest-quality devices based on homoepitaxy-grown thin films. The direct band gap is prohibited due to the material's parity of approximately 2.7 eV, and low-lying CBM, allows for both transparency and conductivity, making it an ideal candidate for transparent contacts. Additionally, the effective electron mass of the material falls between 0.2 and 0.3 times the free electron mass.

REFERENCE

[1] Liang, C.., Meng, G., and Lei, Y., Adv. Mater., **13**, 1330-1333(2001).
[2] Cheng, G., Yang, W., Wang, W., Zhang, X., & Chen, Y., Appl. Phys. An **85** 233-238 (2006).
[3] Memarian, N., Kameli, P., Hajghassem, H., & Ghasemi, E., "J. Phys. Status Solidi C 7 (2010) pp. 2277-2280.
[4] Golshahi, S., Ghafoori-Fard, H., & Askari, M., "Thin Solid Films 518 (2009) pp. 1149-1153.
[5] Boycheva, S., Abrashev, M. V., Harizanova, A., & Popov, T., "Thin Solid Films 515 (2007) pp. 8469-8472.
[6] Lee, J. S., & Choi, W-S., J. Korean Phys. Soc. 64 (2014) pp. 701-705.
[7] Ma, Q., Yu, X., Guo, X., Cheng, Y., Liu, Q., Zhao, J., Wang, Y., & Zhang, S., Nanoscale Res. Lett. 13(4) (2018) Article 135, pp. 1-8.

[8] Horprathum, M., Limsuwan, P., & Phokharatkul, D., Proceedings of the 5th International Conference on Information Technology and Electrical Engineering (ICITEE) (2013) pp. 271-274.
[9] Zhou, J. Ph.D. Thesis. Yale University, 2005, pp. 1-198.
[10] Socol, M., Preda, N., Petre, G., Costas, A., Rasoga, O., Popescu-Pelin, G., Mihailescu, A., Stanculescu, A., and Socol, G., Coatings, vol. 10, no. 10, (2020) pp. 956.
[11] Yahiaa, A., Attafa, A., Saidia, H., Dahnouna, M., Khelifia, C., Bouhdjera, A., et al Surfaces and Interfaces, vol. 14, (2019) pp. 158-165.
[12] Ruzgar, S., Caglar, Y., and Caglar, M., J. Mater. Sci.: Mater. Electron., vol. 31, (2020) pp. 11720-11728.
[13] Lee, J.-Y., Lee, S.-S., Oh, S.-W., Lee, H.-H., Seo, Y.-H., Ryu, B.-H., et al., J. Mater. Chem., vol. 21, 2011, pp. 17066.
[14] Street, R. A., Ng, T. N., and Lujan, R. A., ACS Applied Materials & Interfaces, vol. 6, (2014) pp. 4428-4437.
[15] Ghosh, S. S., Biswas, P. K., and Neogi, S., Solar Energy, vol. 109, (2014) pp. 54-60. DOI: 10.1016/j.solener.2014.08.020.
[16] Hossain, M. A., Khatiwada, D., Paudel, N. R., Chu, C. H., and Kim, K. HJournal of Materials Chemistry A, vol. 3, (2015) pp. 4147-4154. DOI: 10.1039/C4TA05783J.
[17] Horprathum, M., Eitssayeam, S., Sriprapha, K., and Patthanasetakul, V., AIP Conference Proceedings, vol. 2014, (2014) pp. 617-7. DOI: 10.1063/1.4897091.
[18] Gwamuri, J., Zhou, Y., Johnson, C., Green, M., Sabau, A., Cheng, G., and Elangovan, A., Materials, vol. 9, (2016) pp. 63. DOI: 10.3390/ma9010063.
[19] Chang, T. H., Wang, J. C., Liu, Y. H., Cheng, Y. C., Chang, C. Y., Hsu, C. H.,and Chuang, R. W., IEEE Photonics Technology Letters, vol. 27, (2015) pp. 915-918. DOI: 10.1109/LPT.2015.2400446.
[20] Cindemir, U., Lansaker, P. C., Osterlund, L., Niklasson, G. A., and Granqvist, C. G., Coatings, vol. 6, (2016) pp. 19. DOI: 10.3390/coatings6020019.
[21] Luceño-Sánchez, J. A., Díez-Pascual, A. M., and Capilla, R. P., International Journal of Molecular Sciences, vol. 20, (2019) pp. 976
[22] Qurashi, A., Irfan, M. F., and Alam, M. W., The Arabian Journal for Science and Engineering, vol. 35, no. 1C, (2010) pp. 142.
[23] Aquino, A., Paschoalin, V.M.F., Tessaro, L.L.G., Raymundo-Pereira, P.A., and Conte-Junior, C.A., J. Pharm. Biomed. Anal., vol. 202, (2022) pp. 114608.
[24] Twyman, N.M., Tetzner, K., Anthopoulos, T.D., Payne, D.J., and Regoutz, A., Appl. Surf. Sci., vol. 479, (2019) pp. 974-979.
[25] Wang, C., Zeng, H., Liu, K., Lin, Y., Yang, H., Xie, X., Wei, D., and Ye, J.-W., Smart Mater. Med., (2022) pp. 1-10.
[26] Boroujerdi, R. and Paul, R., Chemosensors, vol. 10, no. 2, (2022) pp. 42.
[27] Tandon, B., Gibbs, S.L., Dean, C., and Milliron, D.J., ACS Nano, vol. 16, no. 2, (2022) pp. 1747-1753.
[28] Muydinov, R., Steigert, A., Wollgarten, M., Michaowski, P.P., Bloeck, U., Pflug, A., Erfurt, D., Klenk, R., Körner, S., Lauermann, I., and Szyszka, B., Materials, vol. 12, no. 2, (2019) pp. 266-274.
[29] Chen, M., Cui, D., Zhao, Z., Kang, D., Li, Z., Albawardi, S., Alsageer, S., Alamri, F., Alhazmi, A., Amer, M.R., and Zhou, C., Nano Res., vol. 15, no. 6, (2022) pp. 5510-5516.
[30] Lin, C.F., Kao, C.H., Lin, C.Y., Liu, C.S., and Liu, Y., Sci. Rep., vol. 9, no. 1, (2019) pp. 1-10.
[31] Liu, Q., Zhang, X., Li, J., Wang, W., Liu, Y., Li, B., Chen, J., Li, W., Li, J., and Li, L., iScience, vol. 23, no. 9, (2020) pp. 101469.
[32] Huang, Q., Chen, W., Zhou, X., Zhang, Y., and Zhou, L., in 2015 International Conference on Materials, Environmental and Biological Engineering, Atlantis Press, (2015) pp. 69-72.
[33] Liu, Q., Zhang, X., Li, J., Liu, Y., Wang, W., Li, B., Chen, J., Li, W., Li, J., and Li, L., ACS Nano, vol. 12, no. 2, (2018) pp. 1170-1178.
[34] Aroonyadet, N., Han, D., Li, C., Xu, K., Li, K., Wang, K., and Wang, Z.L., Nano Letters, vol. 15, no. 3, (2015) pp. 1943-1951.
[35] Hossieny Ibrahim, Y. Temerk, and N. Farhan, Talanta, vol. 179, (2018) pp. 75-85.
[36] Weijia Xu, T. Liu, Y. Wang, W. Zhang, X. Yao, B. Hou, Y. Xie, Z. Chu, and Wanqin Jin, Electroanalysis, vol. 33, no. 7, (2021) pp. 1810-1818.
[37] Peng Yang, H. Rong, Z. Wu, and Yanli Pei, IEEE Transactions on NanoBioscience, vol. 20, no. 3, (2021) pp. 287-290.
[38] Mohammed Sedki, Y. Chen, and A. Mulchandani, Sensors, vol. 20, no. 17, (2020) p. 4811.
[39] Rim and Y. Seung, Journal of Information Display, vol. 21, no. 4, (2020) pp. 203-210.
[40] Riccarda Antiochia, Microchimica Acta, vol. 187, no. 12, (2020) pp. 1-13.
[41] Amen, M. T., Pham, T. T. T., Cheah, E., Tran, D. P., and Thierry, B., Molecules, vol. 27, no. 22, (2022) pp. 7952.
[42] Zhu, Z., Yasui, T., Liu, Q., Nagashima, K., Takahashi, T., Shimada, T., Yanagida, T., and Baba, Y., Micromachines, vol. 12, no. 6, (2021) pp. 642.
[43] Amu-Darko, Jesse Nii Okai, Shahid Hussain, Qiang Gong, Xiangzhao Zhang, Ziwei Xu, Mingsong Wang, Guiwu Liu, and Guanjun Qiao. "Highly sensitive In2O3/PANI nanosheets gas sensor for NO2 detection." Journal of Environmental Chemical Engineering 11, no. 1 (2023): 109211.
[44] Amu-Darko, Jesse Nii Okai, Shahid Hussain, Xiangzhao Zhang, Asma A. Alothman, Mohamed Ouladsmane, M. Tariq Nazir, Guanjun Qiao, and Guiwu Liu. "Metal-organic frameworks-derived In2O3/ZnO porous hollow nanocages for highly sensitive H2S gas sensor." Chemosphere 314 (2023): 137670.
[45] Zhang, Su, Shupeng Sun, Baoyu Huang, Nan Wang, and Xiaogan Li. "UV-enhanced formaldehyde sensor using hollow In2O3@ TiO2 double-layer nanospheres at room temperature." ACS Applied Materials & Interfaces 15, no. 3 (2023): 4329-4342.
[46] Bai, Yang, Haitao Fu, Xiaohong Yang, Shixian Xiong, Song Li, and Xizhong An. "Conductometric isopropanol gas sensor: Ce-doped In2O3 nanosheet-assembled hierarchical microstructure." Sensors and Actuators B: Chemical 377 (2023): 133007.

[47] Wang, Shi Kun, Ao Chen Wang, Chao Yue Zhang, Qian Yu Liu, Jun Di Cheng, Yan Chun Wang, Xiu Ping Gao et al. "Sandwich-Structured In2S3/In2O3/In2S3 Hollow Nanofibers as Sensing Materials for Ethanol Detection." ACS Applied Nano Materials 6, no. 4 (2023): 2625-2635.